# Magnetic dot arrays modeling via the system of the radial basis function networks

Denis Horváth [a], Martin Gmitra [a] and Ivo Vávra[b]
[a] Department of Theoretical Physics and Geophysics,
University of P.J.Šafárik,
Moyzesova 16, 040 01 Košice,
Slovak Republic
[b] Institute of Electrical Engineering SAS,
Dúbravská cesta 9, 84239 Bratislava,
Slovak Republic

**Abstract**

Two dimensional square lattice general model of the magnetic dot array is introduced. In this model the intradot self-energy is predicted via the neural network and interdot magnetostatic coupling is approximated by the collection of several dipolar terms. The model has been applied to disk-shaped cluster involving 193 ultrathin dots and 772 interaction centers. In this case among the intradot magnetic structures retrieved by neural networks the important role play single-vortex magnetization modes. Several aspects of the model have been understood numerically by means of the simulated annealing method.

## 1 Introduction

In the recent years there is a remarkable progress in the technology of the nanofabrication of well defined magnetic materials. The material nanoscience based on the epitaxial and lithographic techniques [1] allows the fabrication of the regular arrays of the magnetic particles-dots of well controlled and interesting shape [2], lattice geometry and composition. The increasing technological flexibility calls for further physical ideas, which should be incorporated into design of the artificial nanoscale magnetic systems.

The uniformity of the polarization is the general basic aspect discussed in the connection with the small magnetic particles. The concept of uniformly polarized particle is justified only for the particles of an intermediate size [3, 4]. In the theory [5] the magnetostatic coupling was derived for the homogeneously polarized and saturated cylindrical dots on a rectangular lattice. More restrictive are conditions of the simulation [6], where

each dot of array is substituted by a single dipolar moment. This approximation can be used only for monodomain dots separated by a sufficiently large distances. When a dot array is represented by a system of the interacting dipoles, the search for the ground state configuration leads to the formulation typical for the classical dipolar lattices [7, 8, 9]. The violation of the intradot homogeneity stems from the competition between the magnetostatic, anisotropy and exchange energy terms. The analytical model of the dot array going towards the non-uniformity was proposed in [10]. In this model the interactions of dots were described by the quadrupolar terms.

The problem of the calculation of the magnetization field of a dot array can be in principal formulated in the terms of classical micromagnetic theory [11]. Due to complexity of the problem, the important role in its treatment will play the numerical simulations. They require the implementation of the sufficiently dense discretization within the each ferromagnetic dot. As usual, the magnetic part of the system can be subdivided into interacting dipoles or grains [12, 13], small ferromagnetic cubes [14] or finite elements [15]. Then the optimum spacing of the mesh nodes is determined by a minimum magnetic length scale (exchange, wall) of the system. For the majority of ferromagnetic materials, the comprehensive micromagnetic description is attained when the size of discretization elements decreases into the nanometer regime [15]. Thus, the simulation of a single ultrathin dot of the micrometer size requires about $10^6$ nodes, although, the qualitative simulations can be realized even for $10^2 - 10^4$ nodes [16, 17]. From this we can conclude that both detailed and truncated micromagnetic description of many-dot array represents rather demanding computational task. We summarize, that principal difficulties of micromagnetic dot array analysis come from: (i) the interplay of the phenomena on the intradot (exchange, domain wall) and external geometric length scales; (ii) complexity of the magnetic structure of the non-uniformly polarized dots; (iii) long-range magnetostatic interdot interactions.

To make the problem of the magnetic ordering of dot arrays tractable by a moderate computer facilities, we have developed method, which works on a much coarser mesh than usual discretization schemes allow (except the adaptive and multigrid methods). Its general idea is the simultaneous simulation of the intradot - micromagnetic and multidot scales. This idea was strongly inspired by the multiscale approach [18]. At the present stage of the project, the multidot part of simulation has been developed separately and the behaviour of the small-intradot scales has been treated only phenomenologically. The approach allows a remarkable increase of the simulation speed, indeed, the price payed to the scale separation is the appearance of additional parameters. The completing of the project needs support of the algorithms of the parameter estimation developed on the basis of the standard micromagnetic simulations. Let us to note that similar problems were solved in a cellular automaton version of the molecular dynamics [19].

In this paper we presented the results of the simulation of magnetic properties of quasi-two-dimensional cluster of ultra-thin magnetic dots on the square lattice. The phe-

nomenological aspect of our model is a variable intradot inhomogeneity. The formalism we developed for this aim has been adopted from the models of the neural networks.

From the point of view of the information theory, the neural networks are continuous, unique mappings constructed from the system of known activation functions. The synaptic weights of these activation functions are adjusted by the training process. The standard problem, which can be effectively solved by the neural networks is the association of the input patterns (in our case inputs are effective magnetic moments) with the desired outputs (magnetic self-energy of dot). There are many applications, where neural networks can be implemented. They allow interpolation of the data generated by the simulations or experiment. The example of the physical application is [20], where neural network was used to fit a complicated analytic potential to the set of ab initio data. In [21], the Hopfield type of the interaction matrix was suggested to simulate the dynamics of the complex protein molecule. The specific magnetic application represents the solution of the magnetic inverse problem [22].

For the purpose to model the variable magnetic intradot inhomogeneity we adopted the theory of the radial basis function networks (RBFN) [24]. The RBFN variant of the neural network was chosen, because its ingredient is a straightforward and explicit estimation of the synaptic weights, which allows more transparent analysis of the physical symmetries.

The aim of the paper is to make general presentation of the model and present some numerical results. The paper is organized as follows: In Section 2 the model of the dot array energy functional is introduced. This Section consists of two parts: in Subsection 2.1 we introduced the general phenomenological concept of the nonuniform magnetization, which utilizes self-energy interpolation by means of RBFN approach. In Subsection 2.2 the interaction between dots is introduced. In Section 3 our method is applied to the ultrathin square dots, where tendency of the formation of the vortex intradot phase prevails. Section 4 provides some details about the implementation of the simulated annealing algorithm to the problem of the total energy minimization. Finally, in Section 5 we bring examples of the numerical simulations.

# 2 Model

## 2.1 Intradot self-energy

The microstate of the system of $N$ magnetic dots is described by $N_{\rm c} - by - N$ effective magnetic moments

$$\mathbf{m}_{in}\,, \qquad i = 1, 2, \ldots, N\,, \qquad n = 1, 2, \ldots, N_{\rm c}\,, \tag{1}$$

which are associated with the magnetization field of dot $\mathbf{M}(x, y)$ via the volume averages

$$\mathbf{m}_{in} = m_{\rm sat}^{-1} \int_{(x,y)\in\triangle_{in}} {\rm d}x\,{\rm d}y\,\mathbf{M}(x, y)\ . \tag{2}$$

The formal integration is performed here over $n$th volume element of $i$th dot labeled as $\triangle_{in}$. The saturation magnetic moment $m_{\rm sat} = I_{\rm s}V_{\rm d}/N_{\rm c}$, where $I_{\rm s}$ is the saturation magnetization of the dot, plays role of the normalization factor in Eq.(2). Thus for the effective magnetic moments we have the bounding

$$m_{in,x}^2 + m_{in,y}^2 \leq 1 \ , \tag{3}$$

where $x$, $y$ subscripts refer to the Cartesian components of the effective magnetic moments $\mathbf{m}_{in} = m_{in,x}\mathbf{e}_x + m_{in,y}\mathbf{e}_y$, where $\mathbf{e}_x$ and $\mathbf{e}_y$ are the Cartesian unit vectors. The "softness" of $\mathbf{m}_{in}$ expressed by Eq.(3) is the important model aspect, which differs from the fundamental Brown's postulate [11]. The reason for this modification is that our model is formulated for sufficiently larger elements than classical micromagnetic approach. The total magnetization per dot per interaction center is given by

$$\mathbf{m} = \frac{1}{N\,N_{\rm c}} \sum_{i=1}^{N} \sum_{n=1}^{N_{\rm c}} \mathbf{m}_{in} \ . \tag{4}$$

The effective moments characterizing $i$th dot inside $N$-cluster are distributed around the dot center $\mathbf{R}_i$ and located at $N_{\rm c}$ positions

$$\mathbf{X}_{in} = \mathbf{R}_i + \mathbf{r}_n \, , \qquad n = 1, 2, \ldots , N_{\rm c} \, , \tag{5}$$

where $\mathbf{r}_n$ are some relative coordinates of the interaction centers. From the assumption that identical dots are arranged into array it follows that system of $\mathbf{r}_n$ vectors is independent of the dot position inside the cluster.

In a quasi-two dimensional systems, where $\mathbf{m}_{in}$ is confined to $x-y$ plane, reduced information about $i$th dot microstate is involved in $2N_{\rm c}$ dimensional row vector

$$\tilde{m}_i \equiv [\, \mathbf{m}_{i1} \, , \, \mathbf{m}_{i2} \, , \, \ldots \, , \, \mathbf{m}_{iN_{\rm c}} \,] \tag{6}$$

$$= \left[ \underbrace{m_{i1,x}, m_{i1,y}}_{\text{center } \mathbf{X}_{i1}}, \underbrace{m_{i2,x}, m_{i2,y}}_{\text{center } \mathbf{X}_{i2}}, \ldots , \underbrace{m_{iN_{\rm c},x}, m_{iN_{\rm c},y}}_{\text{center } \mathbf{X}_{iN_{\rm c}}} \right] . \tag{7}$$

We continue with the construction of relations associating the effective dot moments from Eq.(6) with the corresponding self-energies. Here the intradot self-energy is understood as a part of the total energy, which includes only anisotropy, exchange and intradot magnetostatic energy contributions. The Zeeman term and interdot magnetostatic terms, which do not contribute to the self-energy are defined independently of the neural network part of the model.

The construction of the self-energy formula $E^{\rm self}(\tilde{m}_i)$ is based on a proper choice of the set of special $2\,N_{\rm c}$-dimensional memorized vectors (the input patterns of neural networks)

of the type Eq.(7). The memorized vectors are constructed by putting into row $N_{\rm c}$ two-dimensional vectors $\mathbf{p}_n^{(q)}$

$$\tilde{p}^{(q)} = \Big[\, p_{1,x}^{(q)}, p_{1,y}^{(q)}, p_{2,x}^{(q)}, p_{2,y}^{(q)}, \ldots\,, p_{N_{\rm c},x}^{(q)}, p_{N_{\rm c},y}^{(q)} \,\Big]\,. \tag{8}$$

Here, the superscript $q$ identifies so called feature [23]. In our case it is an integer from the set $\Lambda_Q \equiv \{0, 1, \ldots, Q-1\}$. In the analogy with Eq.(6), the subscripts of $p_{n,x}^{(q)}, p_{n,y}^{(q)}$ run over the interaction centers $\mathbf{r}_n$.

To measure the differences between the configurations we have introduced the Euclidean norm

$$||\,\tilde{m}\,|| = \tilde{m}\cdot\tilde{m}^{\rm T} \tag{9}$$

written here for some magnetic moment $\tilde{m}$ [again encoded via the rule from Eq.(7)]. The superscript T from Eq.(9) denotes the vector transposition.

We start the construction of $E^{\rm self}(\tilde{m}_i)$ by assuming that self-energy is known for $Q$ memorized vectors

$$E^{\rm self}(\tilde{p}^{(q)}) = w^{(q)}\,, \qquad q\in\Lambda_Q\,, \tag{10}$$

where $w^{(q)}$ are free parameters of our model. The quality of the interpolation via RBFN depends on the choice of the basis functions and corresponding weights. Most convenient for our preliminary purposes seems to be the use of Nadaraya-Watson regression estimator [24]. According to this, the self-energy input-output relation can be written

$$E^{\rm self}(\tilde{m}) = \sum_{q=0}^{Q-1} w^{(q)}\,\psi^{(q)}(\tilde{m})\,, \tag{11}$$

where

$$\psi^{(q)}(\tilde{m}) = \frac{\exp\Big(-\dfrac{Q}{d_{\rm max}^2}\,||\tilde{p}^{(q)}-\tilde{m}||^2\Big)}{\displaystyle\sum_{q=0}^{Q-1}\exp\Big(-\frac{Q}{d_{\rm max}^2}\,||\tilde{p}^{(q)}-\tilde{m}||^2\Big)} \tag{12}$$

are radial basis functions $\{\psi^{(q)}(\tilde{m})|,\, q\in\Lambda_Q\}$ satisfying the normalization conditions

$$\sum_{q=0}^{Q-1}\psi^{(q)}(\tilde{m}) = 1\,, \qquad 0\le\psi^{(q)}(\tilde{m})\le 1\,. \tag{13}$$

The dot index of $\tilde{m}$ was omitted whenever the distinctions between the individual dots is unimportant. The choice of the dispersion $d_{\rm max}/(\sqrt{2}\,Q)$ in Eq.(12), where

$$d_{\rm max} \;\equiv\; \max_{q,\,q'\,\in\,\Lambda_Q} ||\,\tilde{p}^{(q)}-\tilde{p}^{(q')}\,|| \tag{14}$$

is consistent with the recommendation [24]. Speaking in terms of the neural networks $\psi^{(q)}(\tilde{m})$ is the activation function, which determines $q-$th neuron's response to a given input $\tilde{m}$ and self-energy parameter $w^{(q)}, q \in \Lambda_Q$ is the optimized weight of the link between the input and output layer of the network.

Having established the formula for the calculation of the self-energy, it is easy to prove that if the systems of the memorized vectors is composed from the conjugate vector pairs $\tilde{p}^{(q)}$, $\tilde{p}^{(q')}$ with the same self-energy parameters

$$\tilde{p}^{(q)} = -\tilde{p}^{(q')}\,, \qquad w^{(q)} = w^{(q')} \tag{15}$$

RBFN self-energy form including the typical combination of terms

$$w^{(q)}\Big(\exp(-(Q/d^2_{\max})\,||\tilde{p}^{(q)} - \tilde{m}||^2) + \exp(-(Q/d^2_{\max})\,||\tilde{p}^{(q)} + \tilde{m}||^2)\Big)$$

posses the reflection symmetry

$$E^{\rm self}(\tilde{m}) = E^{\rm self}(-\tilde{m})\ . \tag{16}$$

To analyze the configuration snapshots generated during the simulation process we have introduced so called feature map $\mathcal{F}$. It associates any pattern vector $\tilde{m}$ with the feature $q^* \in \Lambda_Q$ [24]. The feature $q^*$ identifies the index of a nearest memorized vector $\tilde{p}^{(q^*)}$:

$$\mathcal{F}: \qquad q^* \;=\; \mathcal{F}(\tilde{m})\,, \tag{17}$$

$$||\,\tilde{p}^{(q^*)} - \tilde{m}\,|| \;=\; \min_{q\,\in\,\Lambda_Q} ||\,\tilde{p}^{(q)} - \tilde{m}\,||\,. \tag{18}$$

The classification of the features performed for the whole cluster gives rise to the $N-$component vector $\mathcal{F}(\tilde{m}_1), \mathcal{F}(\tilde{m}_2), \ldots, \mathcal{F}(\tilde{m}_N)$. The information about this vector can be concentrated to the form of the sample averages

$$\overline{n}(q) = \frac{1}{N}\sum_{i=1}^{N} \delta_{q,\mathcal{F}(\tilde{m}_i)}\,, \tag{19}$$

where $\delta$ is the usual Kronecker symbol.

## 2.2 Interdot interactions and interactions with the external field

The standard assumption about the interdot interactions is that they are essentially magnetostatic [5]. By using the concept of the effective moments and interaction centers one can construct easily the interdot interaction potential. For this aim we expressed the energy contribution $E^{\rm c-d}_{ik,j}$ consisting of the dipole-dipole interactions of the effective moment

$\mathbf{m}_{in}$ [located at the $n$th center of $i$th dot at the position $\mathbf{X}_{in}$] with $N_{\rm c}$ effective moments of $j$th dot ($j \neq i$)

$$E^{\rm c-d}_{in,j} = \lambda \sum_{\alpha=x,y} m_{in,\alpha} \sum_{\beta=x,y} \sum_{s=1}^{N_{\rm c}} A_{injs,\alpha\beta}\, m_{js,\beta} \ , \tag{20}$$

where

$$A_{injs,\alpha\beta} \ = \ J_{\alpha\beta}\left(\frac{\mathbf{X}_{in}-\mathbf{X}_{js}}{a}\right), \qquad J_{\alpha\beta}(\mathbf{x}) = \frac{|\mathbf{x}|^2\delta_{\alpha\beta} - 3x_\alpha x_\beta}{|\mathbf{x}|^5}\,. \tag{21}$$

Because $\mathbf{X}_{in}$, $\mathbf{X}_{js}$ are scaled by the lattice spacing $a$, the energy dimension is absorbed into dipolar constant

$$\lambda = \frac{m^2_{\rm sat}}{4\pi\mu_0\,\mu_{\rm r}\,a^3}\,, \tag{22}$$

where $\mu_{\rm r}$ is the relative permeability of the matrix. For the interdot magnetostatic energy of dot pair $(i,j)$ we obtain the expression

$$E^{\rm d-d}_{ij} = \sum_{n=1}^{N_{\rm c}} E^{c-d}_{in,j}\ . \tag{23}$$

The key remaining contribution is the Zeeman energy. For $i$th dot interacting with the external magnetic field $\mathbf{H}$ we obtain

$$E^{\rm H}_i = -m_{\rm sat}\,\mathbf{H}\cdot\sum_{n=1}^{N_{\rm c}}\mathbf{m}_{in}\,. \tag{24}$$

In further, to characterize the external field, we have used the reduced undimensional field $\mathbf{h} = m_{\rm sat}\,\mathbf{H}/\lambda$, its components $h_x = \mathbf{h}\cdot\mathbf{e}_x = h\cos\theta$, $h_y = \mathbf{h}\cdot\mathbf{e}_y = h\sin\theta$ and polar angle $\theta$. The final form of total energy functional is then given by

$$E = \sum_{i=1}^{N}\left\{ E^{\rm self}(\tilde{m}_i) + E^{\rm H}_i + \sum_{j=i+1}^{N} E^{\rm d-d}_{ij} \right\}. \tag{25}$$

The schematic view on its structure is displayed in Fig.1. According to the scheme of the computation, the interacting dots have their counterpart in the interacting RBFN blocks. This aspect makes our formulation close to the concept of the interacting neural networks [25].

# 3 The application to the array of rectangle ultrathin magnetic dots

In the concrete case we have modelled the ultrathin (quasi-two dimensional) rectangle magnetic dots of the square profile $\ell_{\rm d} \times \ell_{\rm d}$ and very small height $(V_{\rm d}/\ell_{\rm d}^2) \ll \ell_{\rm d}$. Each dot is replaced by the four moments $N_{\rm c} = 4$ at the positions $\mathbf{r}_n = (1/4)\ell_{\rm d} \ \Big[ \mathbf{e}_x \cos\left(\frac{\pi}{2}(n-1)\right) + \mathbf{e}_y \sin\left(\frac{\pi}{2}(n-1)\right) \Big]$ (see Fig.2(a)). The magnetic moment of $\triangle_{in}$ element [see Fig.3(b)] maintains the saturation value $m_{\rm sat} = I_{\rm s} V_{\rm d}/4$. After this Eq.(22) modifies to the form $\lambda = V_{\rm d}^2 I_{\rm s}^2/(64\pi\mu_0\mu_{\rm r})$.

We have proposed model including $Q = 11$ memorized patterns (see Table 1) and four desired self-energy parameters

$$w^{(q)} = \begin{cases} \mathcal{E}_0 & \text{for} \quad q = 0\,, \\ \mathcal{E}_{\rm v} & \text{for} \quad q = 1, 2\,, \\ \mathcal{E}_{\rm p} & \text{for} \quad q = 3, 4, 5, 6\,, \\ \mathcal{E}_{\rm d} & \text{for} \quad q = 7, 8, 9, 10\,. \end{cases} \tag{26}$$

The additional parameters of the model are reduction coefficients $\kappa_{\rm v} \leq 1$, $\kappa_{\rm p} \leq 1$, $\kappa_{\rm d} \leq 1$ (Table 1) introduced to modify the size of memorized effective moments. These coefficients describe the deviations of moments from the saturated value. According to Eq.(26) one can introduce four subsets of vectors $\{\tilde{p}^{(0)}\}$, $\{\tilde{p}^{(1)}, \tilde{p}^{(2)}\}$, $\{\tilde{p}^{(3)}, \tilde{p}^{(4)}, \tilde{p}^{(5)}, \tilde{p}^{(6)}\}$, $\{\tilde{p}^{(7)}, \tilde{p}^{(8)}, \tilde{p}^{(9)}, \tilde{p}^{(10)}\}$. Within to each subset, the vectors correspond to the same self-energy. This system includes the vector pairs of the opposite sign $p^{(2)} = -p^{(1)}$, $p^{(5)} = -p^{(3)}$, $p^{(6)} = -p^{(4)}$, $p^{(9)} = -p^{(7)}$, $p^{(10)} = -p^{(8)}$ and zero memorized vector $\tilde{p}^{(0)}$. This structure guarantee the reflection symmetry of the self-energy given by Eq.(16).

The exceptional vector $\tilde{p}^{(0)}$ concerns the integral information from multidomain or chaotic magnetization modes of the oscillatory or chaotic character [1]. Its occurrence is a signature of uncertainty in description of a high momentum magnetization modes. Among the patterns memorized and restored by RBFN, we focussed attention to the vortex magnetization modes [1, 26, 27, 28]. The next two vectors $\tilde{p}^{(1)}$ ,$\tilde{p}^{(2)}$ encode the symmetric vortex and counter-vortex configurations in Fig.3(c), Table 1. Similarly, as in the case of $\tilde{p}^{(0)}$, the total magnetic moment of the symmetric memorized vortex is zero. For the rectangular ultrathin isolated dots of square profile and small crystalline anisotropy, the vortex type of magnetic ordering was revealed by the Monte-Carlo simulations [26]. This finding was confirmed by the experiments [27, 28]. Vortex modes were also detected by the simulations on a cubic particles [14] for a weak or zero external magnetic fields. The system of vectors $\{\tilde{p}^{(3)}, \tilde{p}^{(4)}, \tilde{p}^{(5)}, \tilde{p}^{(6)}\}$ belonging to the Stoner-Wohlfart type of single-domain particle [11] is represented by the four parallel effective moments. This ordering can also occur by virtue of the external magnetic or magnetostatic fields. The remaining intradot configurations labeled by $q = 7, 8, 9, 10$ should be the potential sources of (shape)

Table 1: The list of eleven memorized configurations of the magnetic moments $\tilde{p}^{(q)}$ with the corresponding self-energy parameters. The minus sign in $\tilde{p}^{(q)}$ substitutes $-1$.

| $q$ | $\tilde{p}^{(q)}$ | $\mathcal{E}^{(q)}$ |
|---|---|---|
| 0 | $\tilde{p}^{(0)} =$  $= \quad (0,\, 0,\, 0,\, 0,\, 0,\, 0,\, 0,\, 0,\, 0\,)$ | $\mathcal{E}_0$ |
| 1 | $\tilde{p}^{(1)} =$  $= \kappa_{\rm v}\,(0,\, 1,\, -,0,\, 0,\, -,1,\, 0)$ | $\mathcal{E}_{\rm v}$ |
| 2 | $\tilde{p}^{(2)} =$  $= \kappa_{\rm v}\,(0,\, -,1,\, 0,\, 0,\, 1,\, -,0)$ | |
| 3 | $\tilde{p}^{(3)} =$  $= \kappa_{\rm p}\,(0,\, 1,\, 0,\, 1,\, 0,\, 1,\, 0,\, 1)$ | $\mathcal{E}_{\rm p}$ |
| 4 | $\tilde{p}^{(4)} =$  $= \kappa_{\rm p}\,(-,0,\, -,0,\, -,0,\, -,0)$ | |
| 5 | $\tilde{p}^{(5)} =$  $= \kappa_{\rm p}\,(0,\, -,0,\, -,0,\, -,0,\, -)$ | |
| 6 | $\tilde{p}^{(6)} =$  $= \kappa_{\rm p}\,(1,\, 0,\, 1,\, 0,\, 1,\, 0,\, 1,\, 0)$ | |
| 7 | $\tilde{p}^{(7)} =$  $= \kappa_{\rm d}\,(0,\, 1,\, -,0,\, 0,\, 1,\, -,0)$ | $\mathcal{E}_{\rm d}$ |
| 8 | $\tilde{p}^{(8)} =$  $= \kappa_{\rm d}\,(0,\, -,-,0,\, 0,\, -,-,0)$ | |
| 9 | $\tilde{p}^{(9)} =$  $= \kappa_{\rm d}\,(0,\, -,1,\, 0,\, 0,\, -,1,\, 0)$ | |
| 10 | $\tilde{p}^{(10)} =$  $= \kappa_{\rm d}\,(0,\, 1,\, 1,\, 0,\, 0,\, 1,\, 1,\, 0)$ | |

anisotropy. Let us to note that RBFN approach is not sensitive to the physical nature of the anisotropy.

The principal question arises how to determine seven single-dot parameters $\kappa_{\rm v}$, $\kappa_{\rm p}$, $\kappa_{\rm d}$, $\mathcal{E}_0$, $\mathcal{E}_{\rm v}$, $\mathcal{E}_{\rm p}$ and $\mathcal{E}_{\rm d}$. Further work is needed to combine the present simulations with the micromagnetic approaches (see e.g.[16, 29]) incorporating the algorithms of the neural network learning [24]. In this paper the magnetic configurations were selected and parametrized in heuristic manner.

# 4 The implementation of simulated annealing method

Simulated annealing [30] is an optimization technique which operates in a manner analogous to the physical process of annealing. In this section we discuss some details of its implementation to dot array model. The subject of minimization is energy functional Eq.(25) of the effective magnetic moments. The main parts of adopted algorithm are:

**1.** *Initial state* $\tilde{m}_i(t=0)$ is generated (or read from the data file).

**2.** *Cooling schedule.* The pseudotemperature $T(t) = T_0 \, \exp\left(-t/t_0\right))$ relaxes as a function of the discrete time $t = 0, 1, \ldots, t_{\max}$.

**3.** *The update equation* is based on the standard algorithm of Metropolis [31, 32].

**3.1** *Single moment moves.* The lattice dot index $i \in \{1, 2, \ldots, N\}$, and interaction center index $n \in \{1, 2, \ldots, N_{\rm c}\}$ are chosen randomly. At given time $t$, the current effective moment $\mathbf{m}_{in}(t)$ undergoes the stochastic single-moment move $\mathbf{m}_{in}^{\rm trial}(t+1) = \mathbf{m}_{in}(t) + v_{\rm m}\,\mathbf{Y}(t)$, where $\mathbf{Y}$ is two-dimensional vector generated over uniform distribution in $< -1, 1 > \;\times\; < -1, 1 >$. The generation is repeated until the constrain $|\mathbf{m}_{in}(t) + v_{\rm m}\,\mathbf{Y}(t)| \leq 1$ is satisfied; $v_{\rm m}$ is the parameter, which controls the remagnetization speed $|\mathbf{m}(t+1) - \mathbf{m}(t)| \leq v_{\rm m}\,/(N\,N_{\rm c})$. The encoding of $\mathbf{m}_{in}^{\rm trial}(t)$ gives rise to the row vector $\tilde{m}_i^{\rm trial}$(t). By taking into account Eq.(25) with the concrete form of the Nadaraya-Watson self-energy estimator [Eq.(11)] and expression for dipole-dipole interaction Eq.(20) we obtained for the energy variation $\Delta E_{in}$ associated with the elementary move from $\mathbf{m}_{in}(t)$ to $\mathbf{m}_{in}^{\rm trial}(t+1)$ as

$$\Delta E_{in} = \sum_{q=0}^{Q-1} w^{(q)} \left[ \psi^{(q)}(\tilde{m}_i^{\rm trial}) - \psi^{(q)}(\tilde{m}_i) \right] \qquad (27)$$

$$-\lambda \sum_{\alpha=x,y} \left( m_{in,\alpha}^{\rm trial} - m_{in,\alpha} \right) \left[ h_\alpha - \sum_{\beta=x,y} \sum_{j=1, j\neq i}^{N} \sum_{s=1}^{N_{\rm c}} A_{injs,\alpha\beta}\, m_{js,\beta} \right]$$

- *Acceptance criteria* If $\Delta E_{in} \leq 0$, the trial configuration is accepted automatically and $\mathbf{m}_{in}(t+1) = \mathbf{m}_{in}^{\rm trial}(t+1)$. If $\Delta E_{in} > 0$, the trial configuration is accepted if the Boltzmann factor $\exp(-\Delta E_{in}/T)$ is larger or equal to the random number generated uniformly over $< 0, 1 >$.

- *Quasistatic simulations*. In the zero temperature limit, the acceptance criteria reduces to the absolute acceptance if $\Delta E_{in} \leq 0$. For this dynamics the energy is monotonically decreasing function of time. Subsequently, the stochastic motion through the phase space tends to the accessible basin of attraction. In the matastable state the motion gets stuck for a fixed external magnetic field. The sequence of the metastable configurations obtained for a gradually changing external magnetic field was used for the calculation of the quasistatic hysteresis loops.

**3.2** *Complex intradot moves* allows to enhance the effectiveness of annealing and left the metastable states. The update according to **3.1** is supplemented by :

**3.2a** *Interchange moves* changing the location of two intradot configurations: $\tilde{m}_i^{\rm trial} = \tilde{m}_j$, $\tilde{m}_j^{\rm trial} = \tilde{m}_i$ belonging to two randomly chosen dots $i$ and $j$.

**3.2b** *Feature moves* starting with the random choice of the dot index $i$ and its feature $q \in \Lambda_Q$, $q \neq \mathcal{F}(\tilde{m}_i)$. The suggested move is then given by $\tilde{m}_i^{\rm trial} = \tilde{p}^{(q)}$.

**3.2c** *Reflection moves* defined by $\tilde{m}_i^{\rm trial} = -\tilde{m}_i$ are of the special importance since they conserve the self-energy [see Eq.(16)]. Due to this property the simulated system can overcome easily the self-energy barriers.

For the moves **3.2a, b, c** the acceptance probability is given by

$$\min\left\{1, \exp\left(-\sum_{n=1}^{N_{\rm c}} \Delta E_{in}\right)\right\}.$$

**4.** *Stopping criteria*. For $t < t_{\max}$, the annealing process follows from the step **2** with $t \leftarrow t+1$ for the move **3.1**, or with $t \leftarrow t + N_{\rm c}$ in the case of the complex intradot moves **3.2 a, b, c**.

# 5 Numerical simulations

For the model defined in Sect.3 we performed the numerical simulations. We studied finite disk-shaped cluster $R^{\rm cluster} = 8\,a$ including $N = 193$ dots of the size $l_{\rm d} = a/8$. We assume that each dot has $N_{\rm c} = 4$ centers at the square lattice [see Fig.2]. The parameters of memorized magnetic configurations are $\kappa_{\rm v} = \kappa_{\rm d} = 0.95$, $\kappa_{\rm p} = 1$. Consequently, $d_{\max} = 4$.

Table 2: The numerical tests of Nadaraya-Watson formula calculated for two sets of the self-energy parameters. The comparison of desired and retrieved energies [see Eq.(10)]. The formula exhibits weakly non-uniform response $E^{\rm self}(\tilde{p}^{(q\geq 1)})$ to the uniform input $\mathcal{E}^{(q\geq 1)} = 60\lambda$.

| $q$ | $\mathcal{E}^{(q)}/\lambda$ | $E^{\rm self}(\tilde{p}^{(q)})/\lambda$ | $\mathcal{E}^{(q)}/\lambda$ | $E^{\rm self}(\tilde{p}^{(q)})/\lambda$ |
|---|---|---|---|---|
| 0 | 20 | 27.72 | 0 | 25.85 |
| 1, 2 | 0 | 2.84 | 60 | 56.50 |
| 3, 4, 5, 6 | 60 | 55.02 | 60 | 56.88 |
| 7, 8, 9, 10 | 40 | 40.71 | 60 | 56.82 |

The typical parameters of the simulated annealing have been $v_{\rm m} = 0.2$, $t_0 = 200NN_{\rm c}$, $t_{\max} = 5t_0$, and $\lambda = T_0 \leq 10\lambda$. For the quasistatic simulations we used $t_{\max} = 100NN_{\rm c}$.

The initial simulations were performed for a zero external field and zero self-energy parameters. In this case the Monte-Carlo minimization of the energy leads to the rapid fall-off of the energy towards the non-colinear antiferromagnetic chains. The configuration is displayed in Fig.8(a). From this follows that central part of this cluster corresponds to the noncolinear antiferromagnetic phase in agreement with magnetic configuration obtained for a system of cylindrical dots [5] and truncated dipolar moments [9]. At the same time the surface moments which tend to be parallel to the cluster surface exhibit some kind of the frustration [26]. The annealing leads to the ground state estimate $E = E^{\rm AF} = -38.77\lambda N$.

The previous value can be understood as the threshold for the competition between the interdot and intradot structures. The natural way of the stabilization of the intradot vortices is to make the parallel structures of the moments ($q = 3, 4, 5, 6$) energetically unfavorable. In the next we will analyzed more restrictive choice: $w^{(q\neq 1,2)} \geq |E^{\rm AF}|$ with the calibration condition $w^{(q=1,2)} = \mathcal{E}_{\rm v} = 0$.

The previously simulated system was purely magnetostatic. We follow with the simulations of the opposite kind of systems, where interdot interactions have been completely neglected. For these systems we have constructed a quasi-static hysteresis loops. The results have been obtained for the several combinations of the self-energy parameters (comparable with $|E^{\rm AF}|$). They are presented in Figs.4(a)-(d). In Table 2 we list differences between the desired self-energies and outputs of Nadaraya-Watson estimator. Because our parameters are free, the inaccuracy stemming from Nadaraya-Watson formula has no principal significance for the quality of the result. In the situations, where precision of output becomes to be more relevant, the sofisticated RBFN learning is required [24]. The interesting situation has occurred for the self-energy parameters

$$\mathcal{E}_0 = 20\lambda\,, \qquad \mathcal{E}_{\rm v} = 0\,, \qquad \mathcal{E}_{\rm p} = 60\lambda\,, \qquad \mathcal{E}_{\rm d} = 40\lambda \tag{28}$$

corresponding to Fig.4(a). The field dependence of $\overline{n}(q)$ observed during the remagnetiza-

Table 3: The comparing of the several numerical results obtained the external magnetic fields $h = 0$, 5, 10. Table shows structure of energy contributions (divided by $N\lambda$) to the ground state. Calculated for the parameters from Eq.(28).

| energy | $h = 0$ | $h = 5$ | $h = 10$ |
|---|---|---|---|
| total | 1.58 | -3.41 | -11.85 |
| magnetic field | 0.00 | -8.25 | -23.10 |
| self | 6.37 | 13.50 | 24.23 |
| magnetostatic | -4.78 | -8.67 | -12.98 |

tion process for $q = 1, 2$ confirms the vortex stabilization around $h \simeq 0$ and zero remanence. Qualitativelly similar behavior with the vortex annihilation and formation was observed in the experimental study [28]. The situation changes dramatically when the strong interdot interactions are taken into account. Fig.5 shows that their influence causes the non-zero ramanence due to suppression of vortices: $\overline{n}(q) \leq 0.07$ for $q = 1, 2$. More detailed analysis of this fact has revealed that surface vortices are more stable than vortices from the central zones of the cluster. Two next figures 6(a),(b) show how the anisotropy of the memorized configurations is reflected by the hysteresis loops of magnetization components $m_x(h)$, $m_y(h)$ constructed for $\theta = 20^o$.

In the case with the non-zero self-energy parameters interact magnetostatically, the choice of the initial conditions of the simulated annealing becomes to be more complicated. Several final configurations obtained by the annealing process are displayed in Figs.8(b)-(i). The preliminary runs evolving from the initial random state get stuck in the local minimum $E = 6.4\lambda N$. The configuration of this metastable state is displayed in Fig.8(b). The application of the feature map [see Fig.8(c)] reveals that the clustering of the dot states resembles the formation of the homogeneous domains in $Q-$state Potts model [33]. The lowest energy $E = 1.58\lambda N$ was obtained for the system initialized from the vortex state. No essential differences between the pure vortex and mixed vortex-countervortex initial conditions were observed, contrary to our expectation evoked by the study of dipolar system [26]. The question of the helicity will require more detailed investigation. Fig.8(d) shows that magnetostatic deformation of vortices is rather pronounced feature. After the deformation, four-moment vortices acquire the nonzero magnetic moments and resemble the fans or vortices with the non-central Néel-type core. Their analysis via $\mathcal{F}$ map shows the mixing of vortex features $q = 1, 2$ [ $\overline{n}(1) \simeq \overline{n}(2) \simeq 0.5$] and separation of the clusters with different vorticity [see Fig.8(d). This aposteriory finding confirms that parameters of Eq.(28) are sufficient for the stabilization of the vortex ground state for $h = 0$. Two configurations displayed in Figs.8(e),(f) were obtained for the external magnetic field. Their energies are listed in Table 3. For $h = h_x = 5$ the field-deformed vortices resemble

the fans ordered into the large-scale wave-like structures. The waves are better visible from Fig.8(h) showing the detailed snapshot, where intradot magnetic moments are averaged for each dot separatelly. The chaining of field-oriented phase is also visible. For $h = h_x = 10$ Fig.8(i) demonstrates the formation of the clusters with $q = 6$.

To characterize the anisotropy, we have studied the angular dependence of the magnetization for $h = 5$ and varying $\theta \in < 0^o, 180^o >$. In the simulations we have distinguished between the clockwise and counter-clockwise field rotation directions. After the annealing starting from the purely vortex state $\tilde{m}_{1\leq i\leq N}(t = 0) = \tilde{p}^{(1)}$, $\theta = 0^o$ ($\theta = 180^o$) we performed the series of quasistatic remagnetization steps at zero temperature. These simulations have revealed the hard axes $\mathbf{e}_x$, $\mathbf{e}_y$ and easy axes $\mathbf{e}_x \pm \mathbf{e}_y$ [see Fig.7]. In addition, the model system exhibits the angular hysteresis. These results demonstrate how the outputs of RBFN mimic the biaxial anisotropy and how the anisotropy is reinforced by the magnetostatic couplings.

# 6 Conclusions

We believe that very general method we have introduced in this paper will be stimulating for the people working in the field of the micromagnetic simulations of the nanoscale systems. From the point of view of magnetostatics, direct model improvement is possible in many ways: a) near dot interactions can be taken into account more accuratelly by including the rectangle-rectangle magnetostatic terms; b) to speed-up the computations and to extend the system size one can use the hierarchical summation [13]. We thing that more realistic simulations will be possible after the finding of a closer relationship between the neural networks and outputs of the standard micromagnetic approaches.

**Acknowledgement**: This work was supported by the grant no.1/6020/99 and by the Polish-Slovak international grant.

# References

[1] S.Y. Chou, Proceedings of the IEEE 85 (1997) 652.

[2] Te-ho Wu, J.C. Wu, Bing-Mau Chen, Han-Ping D. Shieh, J.Magn.Magn.Mater. 193 (1999) 155.

[3] A. Aharoni, J.Appl.Phys. 68 (1990) 2892.

[4] A. Aharoni, IEEE Trans.Magn. 27 (1991) 4775.

[5] K.Yu. Gushlienko, Appl.Phys.Lett. 75 (1999) 394.

[6] R.L. Stamps and R.E. Camley, J.Magn.Magn.Mater. 177 (1998) 813.

[7] J.M. Luttinger and L. Tisza, Phys.Review 70 (1946) 954.

[8] J.G. Brankov and D.M. Danchev, Physica A 144 (1987) 128.

[9] S. Prakash and C.L. Henley, Phys.Rev. B 42 (1990) 6574.

[10] K.Yu. Gushlienko, "Magnetic anisotropy in dot arrays induced by magnetostatic interdot coupling", to be published in J.Magn.Magn.Mat.

[11] W.F. Brown, "Magnetostatic principles in ferromagnetism", North-Holland Publishing Co. - Amsterdam, Interscience Publishers Inc. - New York, 1962.

[12] D.V. Berkov and N.L. Gorn, Phys.Rev. B 57 (1998) 14332.

[13] J.J. Miles, and B.K. Middleton, J.Magn.Magn.Mater. 95 (1991) 99.

[14] M.E. Schabes and H.N. Bertram, J.Appl.Phys. 64 (1988) 1347.

[15] T. Schrefl, J.Magn.Magn.Mater. 207 (1999) 66.

[16] A.F. Popkov, L.L. Savchenko and N.V. Vorotnikova, Proceedings of the European Conference "Physics of magnetism 99", Poznan 1999, 499.

[17] S. Labbé and P.-Y. Bertin, J.Magn.Magn.Mater. 206 (1999) 93.

[18] F.F. Abraham, J.Q. Broughton, N. Berstein and E. Kaxiras, Computers in Physics 12 (1998) 538.

[19] A. Lejeune, J. Perdang and J. Richert, Phys.Rev.E 60 (1999) 2601.

[20] D.F.R. Brown, M.N. Gibbs and D.C. Clary, J.Chem.Phys. 105 (1996) 17.

[21] L.S. Liebovitch, N.D. Arnold and L. Selector, Journal of Biological systems 2 (1994) 193.

[22] H.V. Jones, A.W.G. Duller, R.W. Chantrell, A. Hoare and P.R. Bissel, J.Magn.Magn.Mater. 193 (1999) 416.

[23] T. Kohonen, "Self-Organizing Maps", Springer, 1995.

[24] S. Haykin, "Neural Networks", by Prentice Hall, Inc. Simon and Schuster/A Viacom Company Upper Saddle River, New Jersey 07458, 1999.

[25] R. Metzler, W. Kinzel and I. Kanter, Phys.Rev.E 62 (2000) 2555.

[26] E.Yu. Vadmedenko, A. Ghazali and J.-C.S. Lévy, Phys.Rev. B 59 (1999) 3329.

[27] T. Shinjo, T. Okuno, R. Hassdorf, K. Shigeto and T. Ono, Science 289 (2000) 930.

[28] A. Fernandez, M.R. Gibbons, M.A. Wall, C.J. Cerjan, J.Magn.Magn.Mater. 190 (1998) 71.

[29] M.R. Scheinfein, J.L. Blue, J.Appl.Phys. 89 (1991) 7740.

[30] S. Kirkpatrick, J.Stat.Phys. 24 (1983) 975.

[31] K. Binder and D.W. Heerman, "Monte Carlo simulation in Statistical Physics", Springer-Verlag, Berlin, New York, 1992.

[32] N. Metropolis, A.W. Rosenbluth, M.N. Rosenbluth, A.H. Teller, and E. Teller, J.Chem.Phys. 21 (1953) 1087.

[33] C. Jeppesen, H. Flyvbjerg and O.G. Mouritsen, Phys.Rev.B 40 (1989) 9070.

## 7 Figure Captions

Figure 1: The schematic view on the calculation of energy functional using RBFN approach: a) the magnetic state of the dot array represented by the system of the eight-dimensional vectors; b) RBFN applied as a predictor of the self-energy output of $i$th dot from the input vector $\tilde{m}_i$; c) the interaction of dots (RBFN) mediated by the effective magnetic moments.

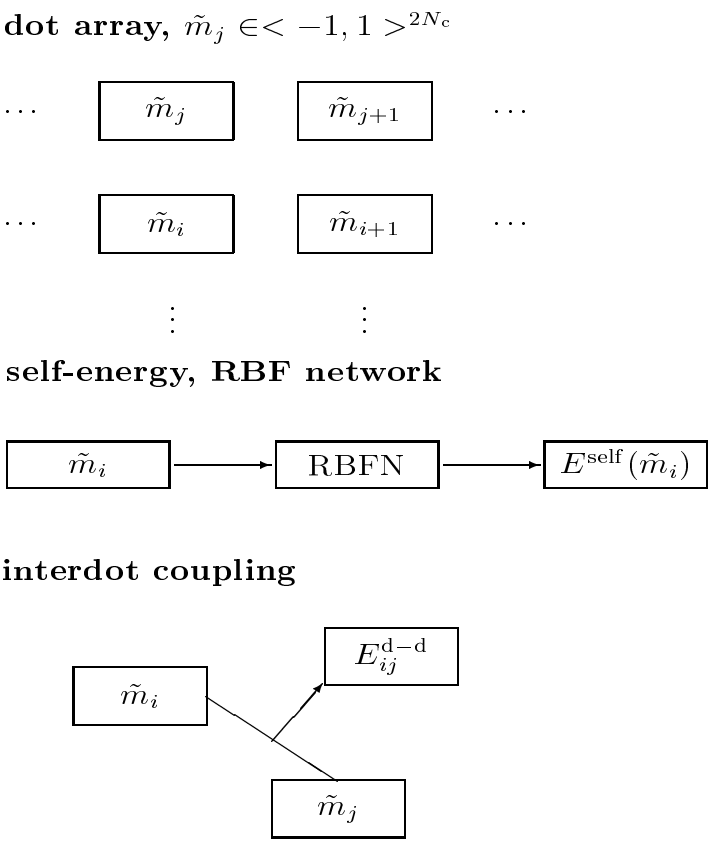

Figure 2: The system of dot centers $\mathbf{R}_1, \mathbf{R}_2, \ldots, \mathbf{R}_{193}$ of the simulated cluster. The unit vectors $\mathbf{e}_x$ and $\mathbf{e}_y$ are parallel to the main directions of the square lattice.

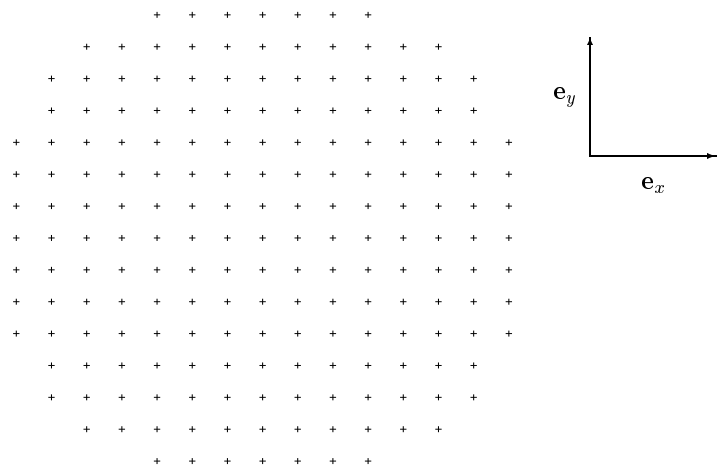

Figure 3: The basic parameters of the dot array model: (a) $i$th dot is located at the position $\mathbf{R}_i$; the magnetic structure of the dot is represented by the four interaction centers and four effective magnetic moments $\mathbf{m}_{in}$; (b) two examples of the dots showing how the effective magnetic moment arises from the integration of the magnetization field over the $\triangle_{in}$ element; (c) the example of the memorized intradot configuration consisting of the four magnetic moments. The example of the encoding of intradot configuration by means of the eight-dimensional vector $\mathbf{p}^{(1)}$.

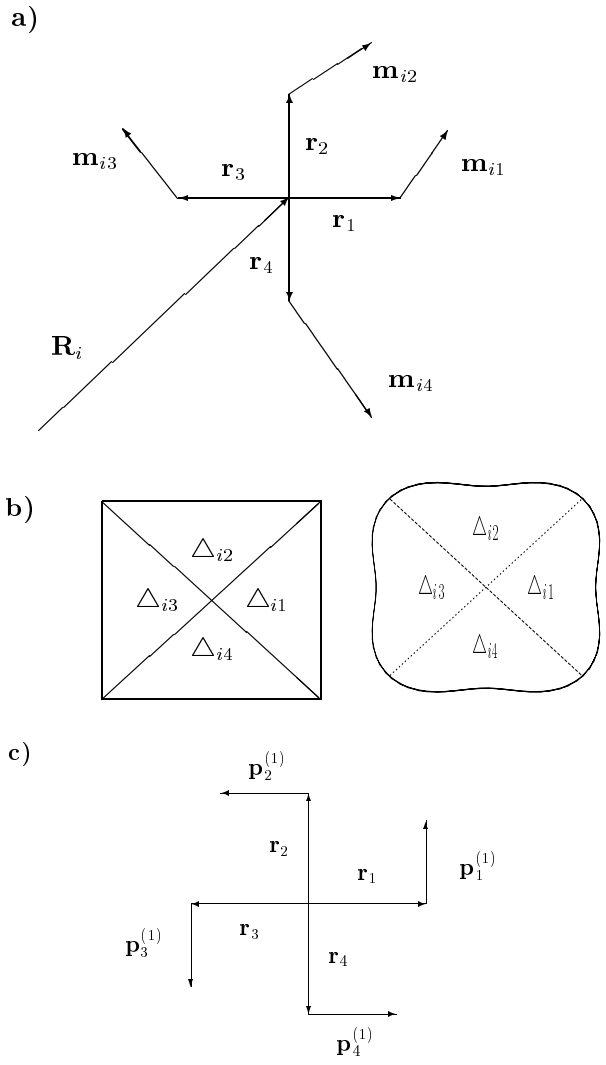

Figure 4: The hysteresis loops of the isolated dots simulated for RBFN parameters: a) see Eq.(28); b) $\mathcal{E}_{\rm v} = 60\lambda, \mathcal{E}_{\rm p} = 0; \mathcal{E}_{\rm d} = 60\lambda, \mathcal{E}_0 = 60\lambda$; c) $\mathcal{E}_{\rm v} = 60\lambda, \mathcal{E}_{\rm p} = 20\lambda, \mathcal{E}_{\rm d} = 0, \mathcal{E}_0 = 60\lambda$; d) $\mathcal{E}_{\rm v} = 0, \mathcal{E}_{\rm p} = 60\lambda, \mathcal{E}_{\rm d} = 60\lambda, \mathcal{E}_0 = 0$.

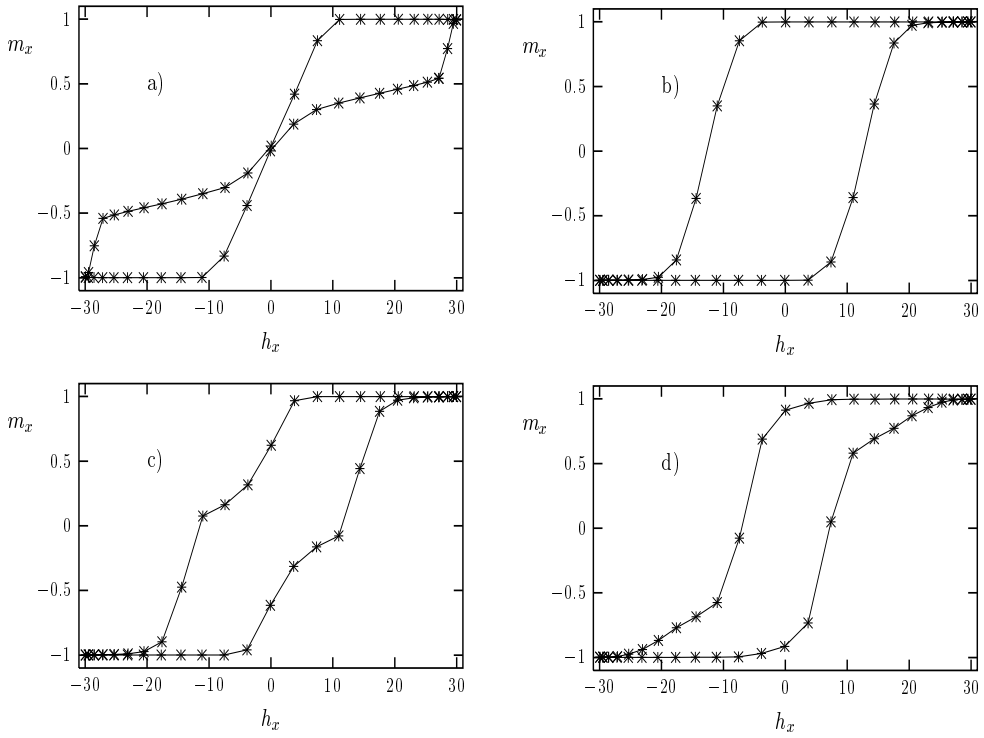

Figure 5: The hysteresis loop of the interacting dots in the anisotropic case, calculated for $\theta = 0^o$ and paramters from Eq.(28).

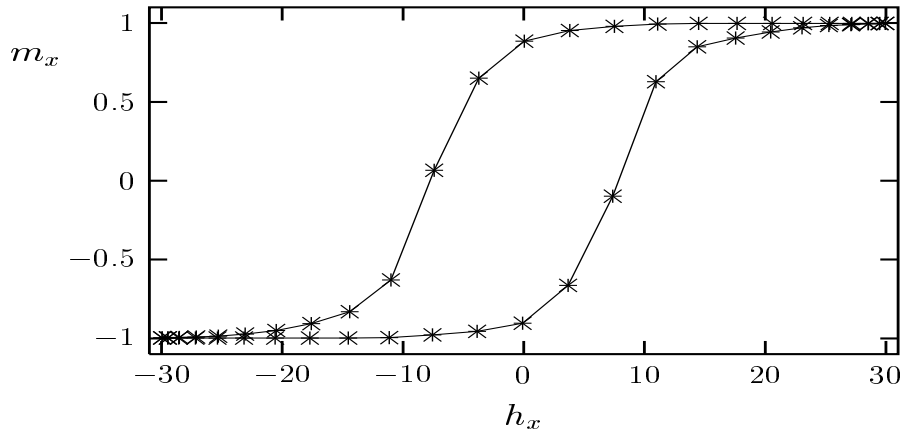


Figure 6: The hysteresis loops of interacting dots in the anisotropic case for $\theta = 20^o$. Calculated performed for the parameters taken from Eq.(28).

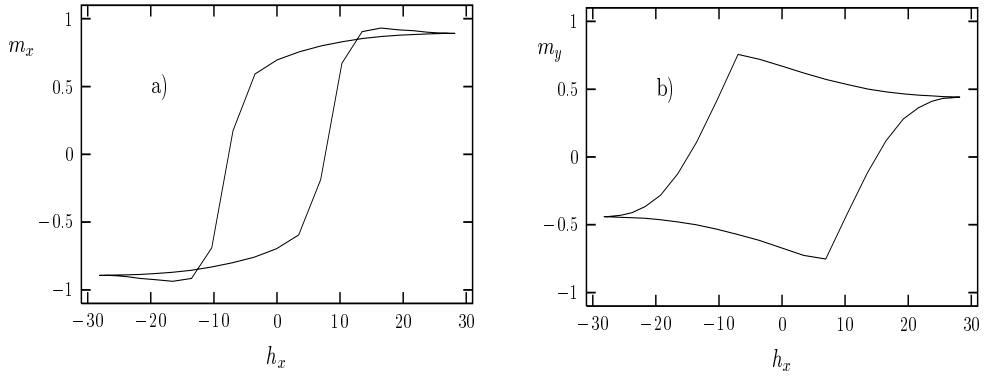

Figure 7: The angular dependence of the magnetization for interacting (int.) and non-interacting (no int.) dot systems confirming the biaxial anisotropy. The arrows indicate direction of the field rotation. Calculated for $h = 5$ and parameters Eq.(28).

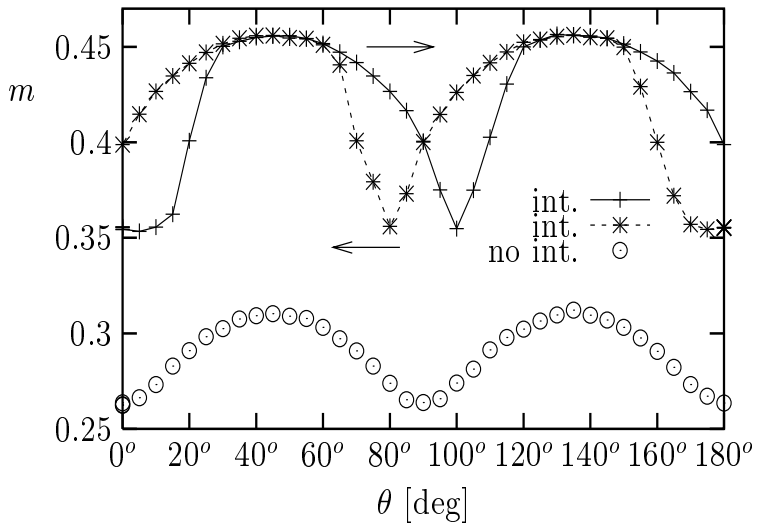

Figure 8: The system of the low energy configurations revealed by the simulated annealing process. The case (a) belongs to the zero self-energy parameters and essentially magnetostatic antiferromagnetic configuration obtained for $h = 0$. The configuration shows only the moments obtained for each dot separatelly. The annealing provides $E = E^{\mathrm{AF}} = -38.77\lambda N$. The results obtained in cases (b)-(i) belong to the parameters from Eq.(28). Part (b) displays disordered - quenched metastable microstate of the energy $E = 6.4\lambda N$ (for $h = 0$) obtained for the random initial condition and forbiden moves **3.2 (a),(b),(c)**. The metadomain structure was analyzed by $\mathcal{F}$ map [case (c)]. The annealing from the initial vortex state stabilizes at the lowest energy $E = 1.58\lambda N$ [cases (d),(g)]. Part (g) shows only the dots with $q = 1$, the remaining part with $q = 2$ was removed for the clearness. For the non-zero external fields we constructed snapshots (e), (h) $h_x = 5$, $h_y = 0$ (wave-like ordered structures); (f), (i) $h_x = 10$, $h_y = 0$ ; Part (h) shows averaged magnetic moments per each dot. It forms wave-like structure. For (i) the formation of $q = 6$ phase clusters is visible (here labels of $q = 1, 2$ features are removed).

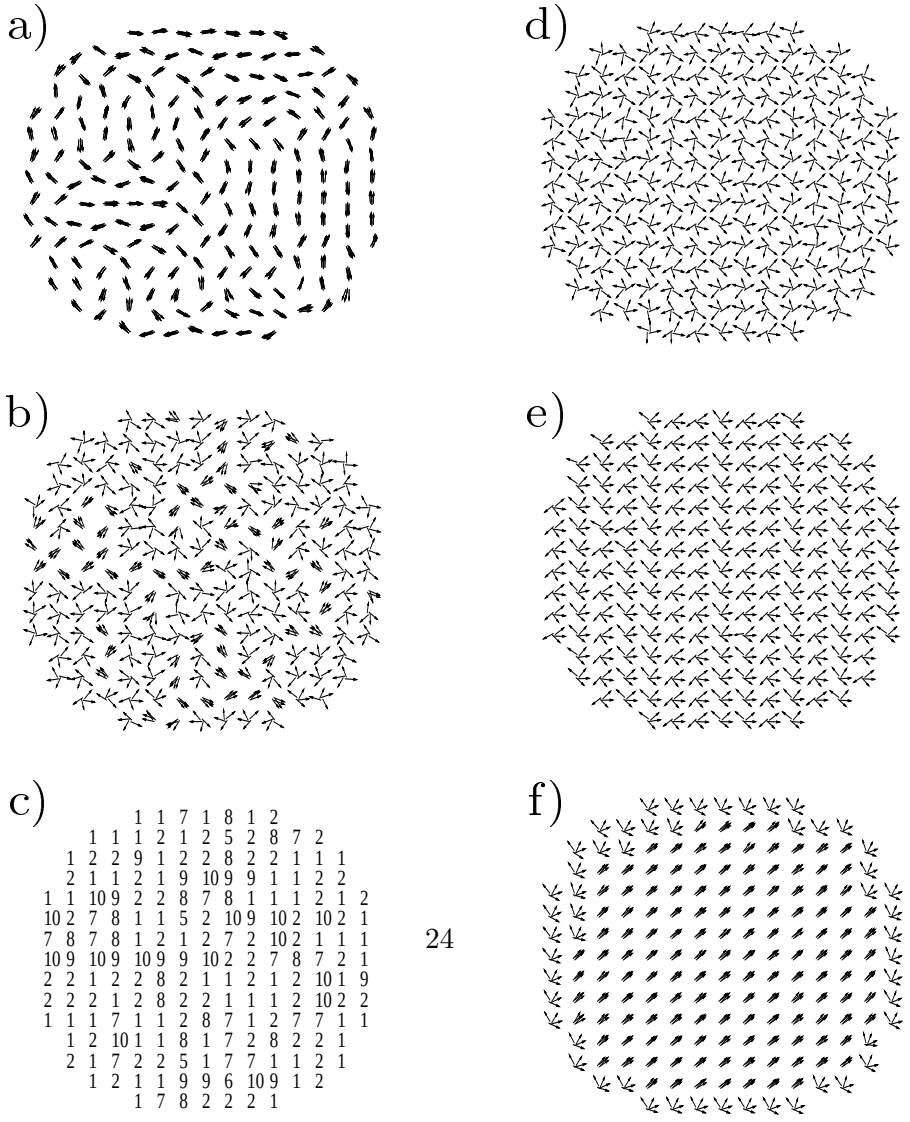

a)

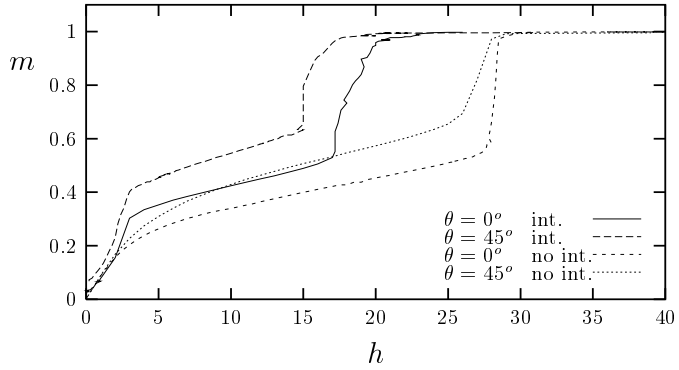


b) $\theta = 45^o$, int.

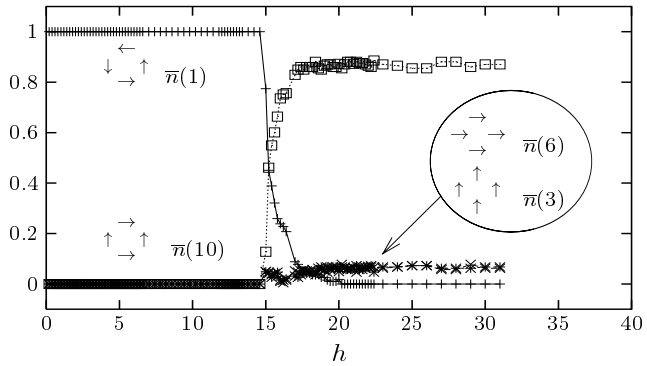

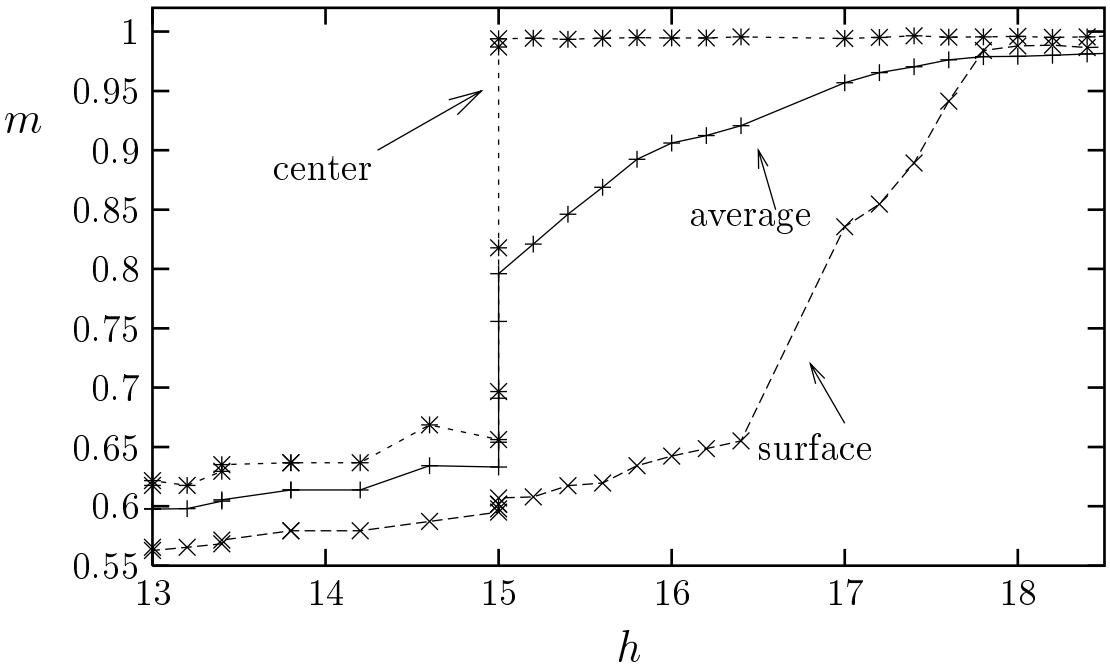
m
h
center
average
surface
1
0.95
0.9
0.85
0.8
0.75
0.7
0.65
0.6
0.55
13
14
15
16
17
18